technologies

MDPI

Article

Comparative Analysis of Multi-Layer and Single-Layer Injection Methods for Offshore CCS in Saline Aquifer Storage

Jiayi Shen [1,2], Futao Mo [1,3], Tao Xuan [4], Qi Li [5,*] and Yi Hong [2,3,*]

[1] Institute of Marine Structures and Naval Architectures, Zhejiang University, Hangzhou 310058, China; jiayi@zju.edu.cn (J.S.); 22334125@zju.edu.cn (F.M.)
[2] Donghai Laboratory, Zhoushan 316021, China
[3] Hainan Institute, Zhejiang University, Sanya 572025, China
[4] CNOOC Energy Development Co., Ltd. Engineering Technology Branch, Tianjing 300450, China; xuantao@cnooc.com.cn
[5] China Energy Engineering Group Zhejiang Electric Power Design Institute Co., Ltd., Hangzhou 310012, China
* Correspondence: qli3194@ceec.net.cn (Q.L.); yi_hong@zju.edu.cn (Y.H.)

Abstract

The aim of this study is to compare the performance of the multi-layer and the single-layer CO_2 injection methods used in offshore carbon capture and storage (CCS) through TOUGH-FLAC numerical simulations. Four key indicators, namely CO_2 saturation, pore pressure, vertical displacement, and Coulomb Failure Stress (*CFS*), are employed as indices to assess the storage capacity of reservoirs and the mechanical stability of caprocks. Numerical simulation results show that the multi-layer injection method increases the CO_2 migration distance and reduces *CFS* values compared with the single-layer injection method. After 1 year of injection, the combined CO_2 migration distance across two aquifers in Case 3 is 610 m, which is greater than that obtained using single-layer injection in Cases 1 and 2 (350 m and 380 m, respectively). Additionally, deep saline aquifers demonstrate superior CO_2 storage capacity due to higher overburden pressure, which also reduces the risk of caprock failures. After 30 years of injection, in Cases 1 and 2, the maximum *CFS* values are 0.591 and 0.567, respectively, and the CO_2 migration distances are 2400 m and 2650 m, respectively. Overall, the findings of this study indicate that the multi-layer injection method, particularly in deep saline aquifers, provides a safer and more efficient CO_2 injection approach for offshore CCS projects.

Keywords: offshore CCS; marine saline aquifers; multi-layer injection; single-layer injection; CO_2 storage capacity

check for updates

Received: 18 July 2025
Revised: 18 August 2025
Accepted: 19 August 2025
Published: 21 August 2025

Citation: Shen, J.; Mo, F.; Xuan, T.; Li, Q.; Hong, Y. Comparative Analysis of Multi-Layer and Single-Layer Injection Methods for Offshore CCS in Saline Aquifer Storage. *Technologies* **2025**, *13*, 375. https://doi.org/10.3390/technologies13080375

Copyright: © 2025 by the authors. Licensee MDPI, Basel, Switzerland. This article is an open access article distributed under the terms and conditions of the Creative Commons Attribution (CC BY) license (https://creativecommons.org/licenses/by/4.0/).

1. Introduction

Carbon capture and storage (CCS) is widely recognized as one of the most effective technologies for reducing CO_2 emissions [1–3]. Among various CCS technologies [4–9], offshore CCS has attracted significant attention because of its massive CO_2 storage capacity and geographic isolation from populated areas.

Offshore saline aquifers, which are widely distributed across continental shelf regions, are considered ideal geological formations for large-scale CO_2 storage [10,11]. These formations typically consist of multi-layered high-permeability reservoirs such as sandstone inter-bedded with low-permeability caprocks such as mudstones or shales, which provide massive storage capacity and safe sealing conditions for long-term CO_2 storage [12]. However, the complex stratigraphy of multi-layer reservoirs and caprocks makes traditional

single-layer CO_2 injection methods insufficient to ensure both reservoir storage efficiency and caprock integrity [13–17]. Therefore, many researchers adopted multi-layer injection techniques, which involve distributing CO_2 across multiple reservoir layers to optimize storage capacity and minimize mechanical stress [18]. Zhu et al. [19,20] carried out numerical simulations to study the mechanical responses of reservoirs and caprocks undergoing multi-layer CO_2 injection in the Shenhua CCUS project. Their studies revealed that CO_2 preferentially migrates through high-permeability layers, leading to faster lateral pressure diffusion, while its migration and pressure transmission are significantly slower in low-permeability layers. Therefore, to maximize the storage capacity of multi-layered reservoirs, it is essential to adjust injection rates based on the permeability of each target layer. Liu et al. [21] used TOUGH2 to study the effects of injection rate, temperature, and boundary conditions on CO_2 migration in multi-layer saline formations, identifying the injection rate as the primary factor influencing CO_2 migration distance. Kivi et al. [22] compared single-layer and multi-layer injection models to assess the safety of CO_2 storage at the gigatonne scale; they found that the risk of CO_2 leakage through a multi-layer reservoir is significantly lower than that in a single-layer reservoir. Wei et al. [23] further reported that the use of the multi-layer injection method results in relatively lower levels of induced seismicity in these formations compared with the single-layer injection method.

Although the existing numerical simulations of CCS projects demonstrated the potential advantages of multi-layer injection, there still remains a lack of systematic comparative studies to evaluate the difference in the CO_2 plume distribution and stability of formations between single-layer and multi-layer CO_2 injection methods. This is particularly important for offshore saline aquifer CCS, where geological conditions are often characterized by multi-layer reservoirs and caprocks.

This study aims to conduct a comparative analysis to evaluate the performance of multi-layer and single-layer CO_2 injection methods used in offshore saline aquifers in the East China Sea Shelf Basin using the TOUGH-FLAC numerical model. Four key indicators, namely CO_2 saturation, pore pressure, vertical displacement, and Coulomb Failure Stress (*CFS*), are used as indices to assess the storage capacity of reservoirs and the mechanical stability of caprocks to provide a safer and more effective approach for large-scale offshore CCS projects.

2. Numerical Model for CCS

2.1. Geological Conditions

The Lishui Sag is located in the East China Sea Shelf Basin (as indicated by the red box in Figure 1a), which is one of the most favorable areas for CO_2 geological storage in China's offshore continental margin basins [24,25]. Since the beginning of the Middle Miocene, the Lishui Sag has undergone a long period of tectonic uplift, forming rich sedimentary strata. The main geological interfaces are shown in Figure 1b. One of the Paleocene sedimentary formations, named the Mingyuefeng Formation, is characterized by high aquifer permeability and low caprock permeability, making it the primary reservoir for gas fields [26–28]. In addition, the Lishui Sag has thick sedimentary strata, stable structures, and particularly developed implicit composite traps controlled by both structure and lithology, which means there is a regional caprock suitable for CO_2 saline aquifer storage.

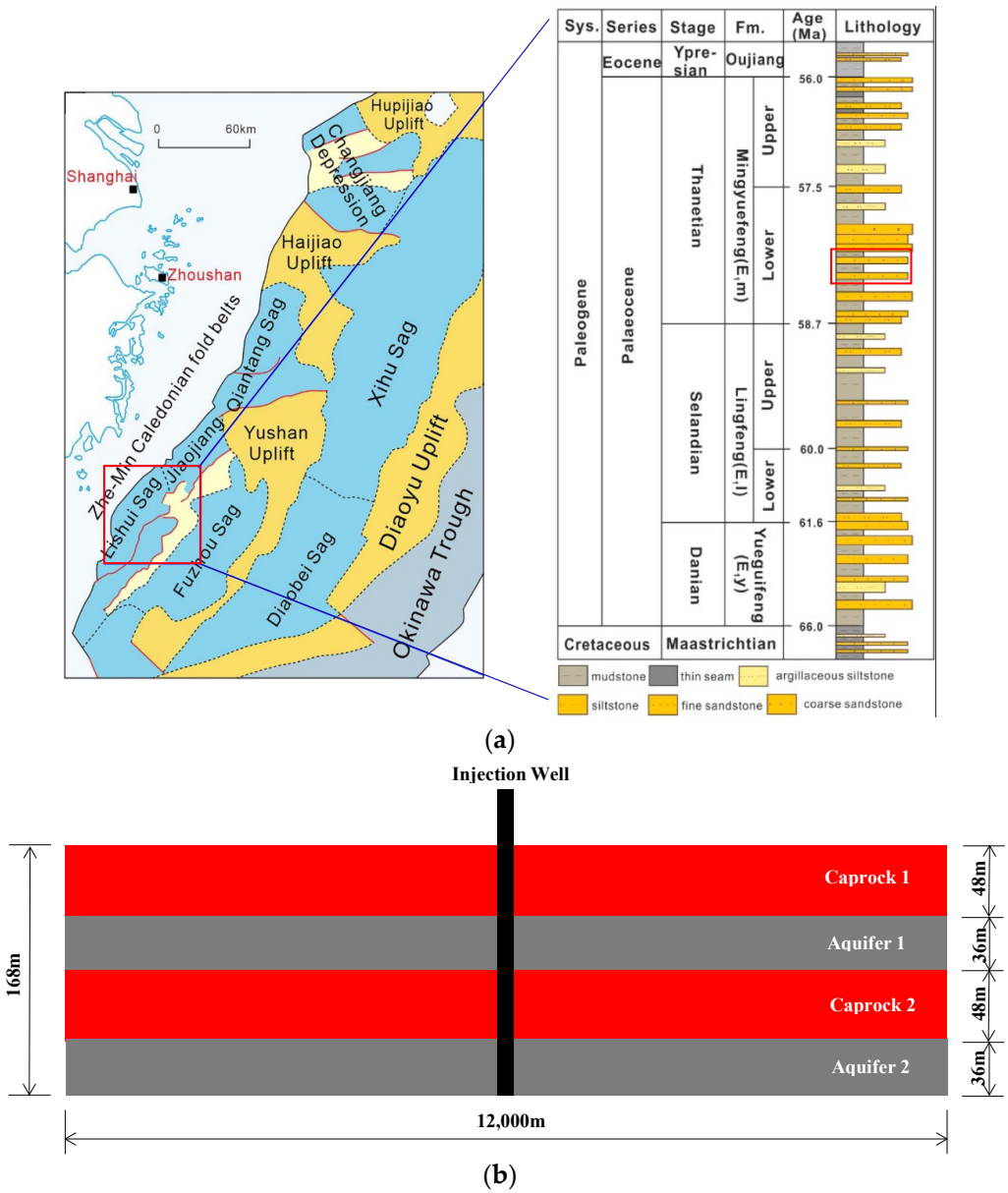


Figure 1. Stratigraphic units of the Paleocene of the Lishui Sag in the East China Sea Shelf Basin. (**a**) Stratigraphic column of Paleocene strata in the Lishui Sag and (**b**) multi-layer CO_2 storage model.

2.2. Numerical Modeling

TOUGH2 is a piece of numerical simulation software for modeling the flow of multiphase fluids in porous or fractured media. FLAC3D 7.0 is a piece of numerical software designed for geotechnical and geomechanical analysis of soil, rock, and other geomaterials. TOUGH-FLAC coupled simulation is a numerical approach used to describe the interaction between underground multiphase fluid flow and geomechanical responses.

The TOUGH-FLAC model has been widely used to simulate the coupled behavior of multiphase fluid flow and geomechanical responses of geological formations for various geological projects [29], such as CO_2 geological storage [30] and geothermal and hydrocarbon extraction [31,32]. Within this coupling framework, TOUGH solves the governing equations for multiphase fluid and heat flow in porous and fractured media based on Darcy's law and conservation principles, enabling simulations of subsurface processes such as CO_2 injection. FLAC, in turn, solves stress-induced deformations and fracture propagation in the formations resulting from fluid injection using the appropriate constitutive models. The two modules are coupled through the iterative exchange of pore pressure and stress-strain

data at each timestep, enabling the simulation of fully coupled hydromechanical processes. This framework allows for an accurate assessment of geomechanical responses induced by fluid injection into formations.

In this study, CO_2 was injected into the Mingyuefeng Formation, which consists of sandstone saline aquifers (reservoirs) and mudstone layers (caprocks), as shown in Figure 1a. A two-dimensional planar multi-layer aquifer and caprock model was established based on the TOUGH-FLAC framework to investigate the interaction between mechanical deformation and fluid flow during CO_2 injection.

The current model does not incorporate geochemical reactions such as mineral dissolution or CO_2 solubility in formation water, even though these mechanisms are critical for long-term CO_2 storage performance. However, the present study specifically focuses on the short-term hydromechanical responses during the injection phase (30 years), in which mechanical stability is predominantly governed by stress changes and deformation rather than by chemical alterations. Under such conditions, the combined use of *CFS*, pore pressure, and vertical displacement is considered sufficient and was adopted in previous CO_2 storage studies [33] for short-term risk evaluation.

The model is 12,000 m long and 168 m thick, and it extends from −2075 to −2243 m. From top to bottom, there are four layers, including two high-permeability aquifers with a thickness of 36 m and two low-permeability caprocks with a thickness of 48 m.

The model parameters are shown in Table 1. The geological and mechanical parameters listed in Table 1 were chosen to be representative of the Paleocene formations in the Lishui Sag, derived from a combination of site-specific core and petrophysical measurements [34] and established literature values for similar lithologies [35,36]. This combination ensures that the model inputs are both geologically representative and suitable for reliable numerical simulation.

Table 1. Stratigraphic parameter values.

Indicators	Parameters *	Value	Units
Caprock			
Poisson's ratio	μ_c	0.27	-
Void ratio	n_c	0.02	-
Young's modulus	E_c	8.11	GPa
Permeability	k_c	1×10^{-17}	m^2
Angle of friction	φ_c	30	°
Dry density	ρ_c	2600	kg/m^3
Cohesion	c_c	1.2	MPa
Aquifer			
Poisson's ratio	μ_r	0.25	-
Void ratio	n_r	0.15	-
Young's modulus	E_r	13.5	GPa
Permeability	k_r	1×10^{-13}	m^2
Angle of friction	φ_r	35	°
Dry density	ρ_r	2600	kg/m^3
Cohesion	c_r	8.2	MPa

* The subscripts "c" and "r" represent the caprock and the aquifer, respectively.

The setting of boundary conditions of the numerical model is shown in Figure 2. Both left and right sides are set as stress boundaries to simulate the situation where the total horizontal stress of the formation is unchanged during CO_2 injection. The vertical stress σ_v on the surface of the model is given by the overlying formation pressure, with a magnitude of 51.91 MPa. The horizontal stress σ_h on the surface of the model is 36.34 MPa, which is approximately 0.7 times the vertical stress σ_v [37], and the gradient with depth is 17.51 kPa/m. The bottom of the model is set as a fixed displacement boundary, limiting the vertical and horizontal displacement of the bottom boundary. The horizontal displacement of the two side boundaries is limited to zero, allowing for vertical displacement.

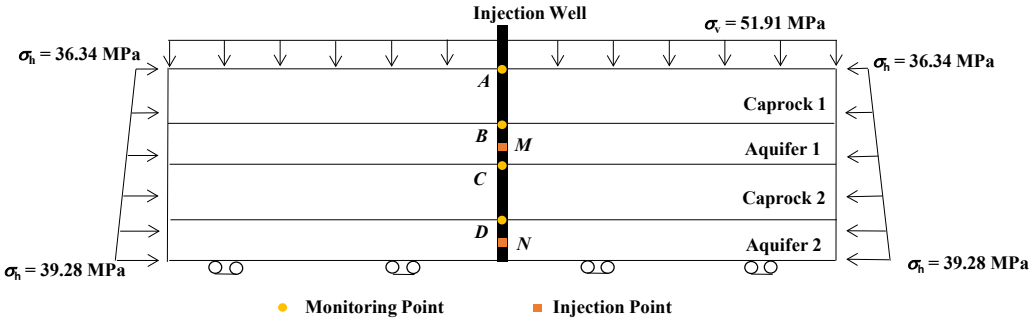


Figure 2. Boundary conditions of the numerical model.

The injection well is located in the center of the model, and monitoring points are located at the top of the four formations, marked as points *A*, *B*, *C*, and *D*, with depths of −2075, −2123, −2159, and −2207 m, respectively. CO_2 injection points are in the middle thickness of the two aquifers, with depths of −2141 and −2225 m, respectively. When the multi-layer CO_2 injection is performed, the total injection rate needs to be assigned to each aquifer. In this study, the injection rate is assigned according to the permeability and thickness of the aquifers. For the total injection rate q, the portion allocated to injection layer i can be calculated according to Equation (1):

$$q_i = \frac{k_i H_i}{\sum_i k_i H_i} q \tag{1}$$

where q_i is the injection flow rate of aquifer i, q is the total flow rate, k_i is the permeability of aquifer i, and H_i is the thickness of aquifer i.

2.3. Evaluation Indicators

Once CO_2 is injected into the aquifer, it migrates upwards and accumulates at the bottom of the caprock. When the accumulated CO_2 saturation reaches a certain threshold, CO_2 begins to displace the aquifer fluid and further diffuse, potentially causing uplift and deformation of the caprock [38]. If the pore pressure of the aquifer exceeds the rupture pressure of the caprock, the interface between the aquifer and caprock is subjected to shear or tension, which can cause hydraulic rupture of the caprock and generate high permeability channels, leading to CO_2 leakage [39,40]. Therefore, in this research, we selected four parameters, namely, CO_2 saturation, pore pressure, vertical displacement, and Coulomb Failure Stress (*CFS*), as indicators to evaluate CO_2 sequestration capacity and site safety. The distribution of CO_2 saturation effectively reflects the migration behavior of CO_2 within aquifers and caprock layers, which is relevant for assessing the safety aspects of geological storage [41]. Pore pressure alters the stress state of rock masses, thereby affecting their mechanical properties, which is essential for an accurate assessment of storage safety and sustainable injection. Vertical displacement serves as an indicator of

formation deformation, significantly influencing the integrity of caprock sealing [33]. The value of *CFS*, as shown in Equation (2), is commonly used to assess rock stability and caprock integrity [42].

$$CFS = \tau/(\mu(\sigma - P) + S) \quad (2)$$

where τ is shear stress, μ is the coefficient of friction, σ is normal stress, P is pore pressure, and S is cohesive force. *CFS* can be regarded as the ratio of the shear stress at the corresponding point on the Mohr circle to the distance from the failure envelope. When $CFS \geq 1$, it indicates that there is a risk of instability and failure at that point. When $CFS < 1$, it indicates that the point is safe.

2.4. Simulation Schemes

This study aims to conduct a comparative analysis of different CO_2 injection schemes in the model and identify the optimal injection scheme. Therefore, three aspects of comparative analysis were carried out: (1) a comparison between single-layer and multi-layer injection methods; (2) a comparison between deep aquifer injection and shallow aquifer injection; and (3) a comparison of different CO_2 injection rates.

Four injection scenarios were designed for numerical simulations. Cases 1 and 2 are single-layer injection methods, injecting CO_2 into Aquifer 1 and Aquifer 2, respectively, at a rate of 3.170 kg/s. Cases 3 and 4 are multi-layer injection methods, injecting CO_2 into Aquifer 1 and 2 simultaneously, with injection rates of 1.585 kg/s and 3.170 kg/s, respectively. Specific injection conditions for each case are listed in Table 2.

Table 2. Case design for numerical simulations.

Case	Injection Method	Injection Rate, (kg/s)		Injection Time, (Year)
		Aquifer 1	Aquifer 2	
1	Single-layer	3.170	0	30
2	Single-layer	0	3.170	30
3	Multi-layer	1.585	1.585	30
4	Multi-layer	3.170	3.170	30

3. CO_2 Saturation

The distribution of CO_2 saturation can reveal the migration of CO_2 in the aquifer and reflect the carbon storage capacity. Therefore, this study compared the CO_2 saturation distribution under different injection cases. Figure 3 shows the saturation distribution of CO_2 under four injection cases after 1, 5, 10, 20, and 30 years. It is found that the process of CO_2 migration in aquifers includes upward migration and horizontal migration. This is because the density of CO_2 is lower than that of aquifer fluids, which leads CO_2 to migrate upward and accumulate at the bottom of the caprock during the initial injection stage. When the pressure created by the accumulation of CO_2 is large enough to drive the fluid flow in the aquifer, the CO_2 will migrate further along the horizontal direction.

Table 3 summarizes the CO_2 migration distance L within the aquifer at 1, 5, 10, 20, and 30 years for the four injection cases illustrated in Figure 3. The value of L is defined as the horizontal distance between the CO_2 diffusion front and the injection point, as shown in the sub-figure of Figure 3 for Case 2 at the 30-year interval (bottom row).

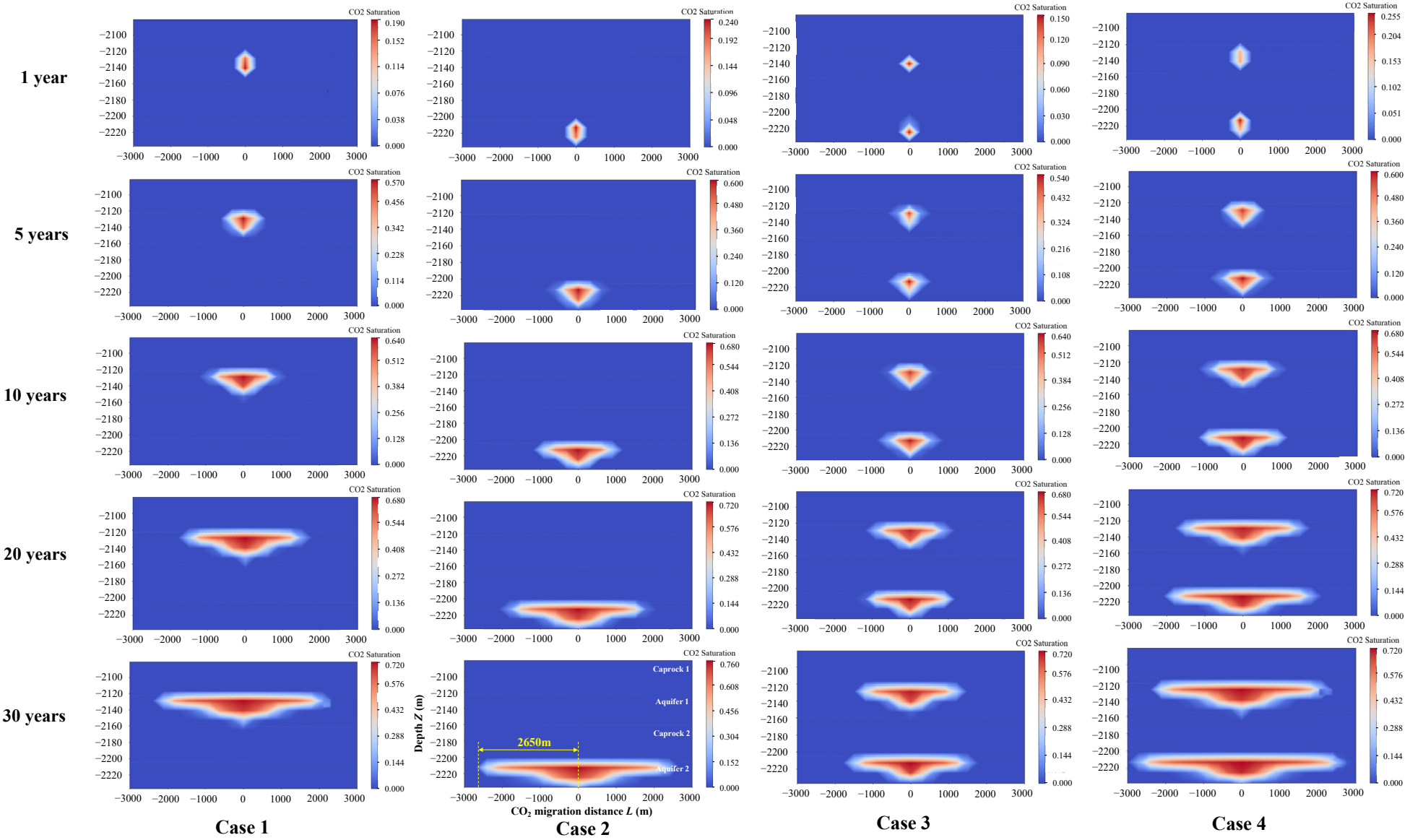


Figure 3. CO_2 saturation distributions under four injection scenarios.

Table 3. The CO_2 migration distances in each aquifer under four injection scenarios.

Case	Aquifer	Injection Rate, (kg/s)	The CO_2 Migration Distances *L*, (m)				
			1 Y	5 Y	10 Y	20 Y	30 Y
1	1	3.170	350	550	1050	1700	2400
	2	0	---	---	---	---	---
2	1	0	---	---	---	---	---
	2	3.170	380	700	1200	2000	2650
3	1	1.585	300	550	800	1200	1500
	2	1.585	310	600	850	1400	1750
4	1	3.170	320	650	1100	1750	2400
	2	3.170	350	800	1250	2100	2900

Although the CO_2 migration distance in each aquifer under the multi-layer injection method (Case 3) is shorter than that in the single-layer injection method (Case 1 or Case 2) when the total injected rate is the same, the combined migration distance across both aquifers in Case 3 is greater than that of Case 1 or Case 2. For example, in Case 3, the migration distances are 300 m in Aquifer 1 and 310 m in Aquifer 2 after 1 year of CO_2 injection, giving a combined total of 610 m, which is greater than that obtained in the single-layer injection scenarios in Cases 1 and 2 (350 m and 380 m, respectively). This broader migration distance allows the multi-layer injection method to utilize more of the available reservoir volume, thereby improving overall storage efficiency.

It can also be concluded that the migration distance of CO_2 in the deeper aquifer is larger than that of the shallower aquifer. For example, after 30 years of injection of Case 3, the values of *L* are 1500 and 1750 m for Aquifer 1 and 2, respectively.

It is well known that CO_2 viscosity increases with depth, which decreases the mobility of CO_2. However, this viscosity effect is offset by the changes in CO_2 density and compressibility, which enhance CO_2 mobility by strengthening the buoyancy- and pressure-driven forces that govern its migration. These combined effects result in an overall increase in CO_2 mobility, which is consistent with previous findings on deep-formation CO_2 storage [43]. As a result, CO_2 migrates more easily in deeper aquifers, making them more favorable for long-term CO_2 storage.

Additionally, the migration distance of CO_2 increases with the increase in injection rates. After 30 years of CO_2 injection, the migration distances in Aquifer 1 for Case 3 and Case 4 are 1500 and 2400 m, respectively. This is because a higher injection rate generates a higher fluid pressure, which facilitates CO_2 migration.

4. Pore Pressure

Pore pressure is a critical indicator for evaluating the safety of CO_2 storage sites. Figure 4 illustrates the variations in pore pressure at the injection point under different injection cases. At the initial stage of CO_2 injection, pore pressure rapidly increases with the increase in injection time and then tends to be stable. This is because CO_2 accumulates extensively beneath the caprock in the early injection phase, causing a rapid increase in pore pressure. As the injection process stabilizes, the pore pressure gradually approaches a steady state. For example, in Case 1 (Figure 4a), the pore pressure at the injection point in Aquifer 1 rises rapidly within the first three years, reaching a peak of 23.31 MPa. Subsequently, the pore pressure decreases slightly to 23.09 MPa by the end of 30 years.

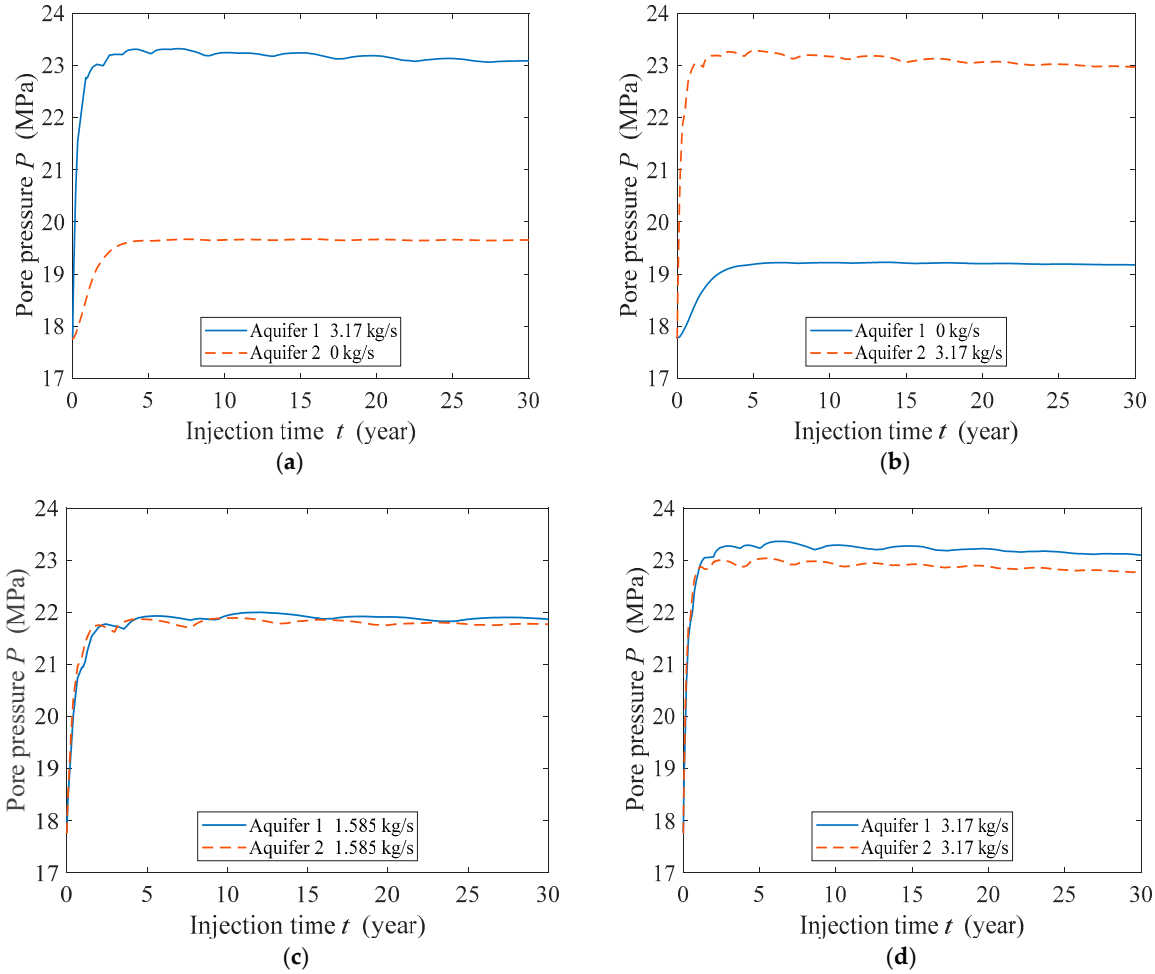


Figure 4. Variations in pore pressure at the injection points. (**a**) Case 1, (**b**) Case 2, (**c**) Case 3, (**d**) Case 4.

Figure 4c,d show that the pore pressure of Aquifer 2 is lower than that of Aquifer 1 during the CO_2 injection processes. This phenomenon occurs because the overburden pressure of deep aquifers is greater than that of shallow aquifers, which means deep aquifers offer better CO_2 storage capacity than shallow aquifers.

Table 4 shows the maximum pore pressure P_{max} in the aquifers under different injection scenarios. It can be observed that the values of P_{max} for Cases 1, 2, and 3 are 23.31, 23.29, and 22.02 MPa, respectively, which indicates that the use of the multi-layer injection method is safer than the single-layer injection method.

Table 4. The maximum pore pressures for each aquifer under four injection scenarios.

Case	Injection Rate, (kg/s)	Aquifer	Maximum Pore Pressure P_{max}, (MPa)
1	3.170	1	23.31
	0	2	19.63
2	0	1	19.22
	3.170	2	23.29
3	1.585	1	22.02
	1.585	2	21.88
4	3.170	1	23.36
	3.170	2	23.03

5. Vertical Displacement

After CO_2 is injected into the aquifer, it migrates upward, generating buoyancy forces that cause vertical displacement of the caprock. Figure 5 shows the vertical displacement at the top of the aquifer after 30 years of injection. It is found that the maximum vertical displacement V_{max} occurs at the injection point, and as the distance from the injection point increases, the vertical displacement of the aquifer decreases. In addition, during the injection process, the vertical displacement of Aquifer 1 is greater than that of Aquifer 2, which indicates that the risk of CO_2 leakage caused by vertical displacement is lower in deep aquifers compared to shallow aquifers, which means deep aquifers are more suitable for CO_2 storage.

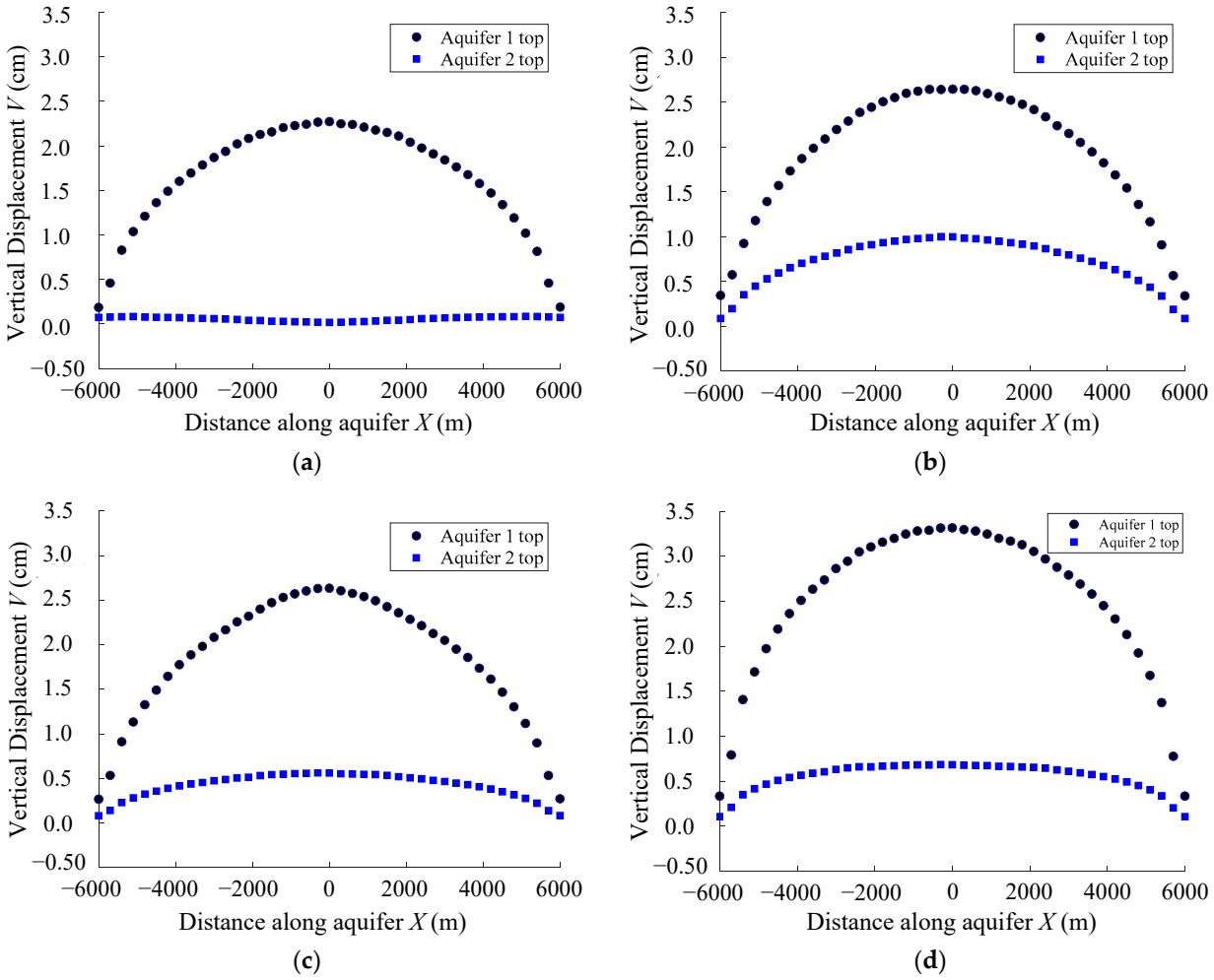


Figure 5. Vertical displacements at the top of the aquifers after 30 years of injection. (**a**) Case 1, (**b**) Case 2, (**c**) Case 3, (**d**) Case 4.

Table 5 summarizes the maximum vertical displacement (V_{max}) for each aquifer during the injection process. The V_{max} values for Cases 1, 2, and 3 are 2.334, 2.840, and 2.683 cm, respectively. According to previous studies, excessive vertical displacement can lead to misalignment at the interface between the injection well and the caprock, potentially creating high-permeability leakage pathways [38]. The simulation results indicate that the CO_2 leakage risk in Case 2 is the highest under the same injection rate of 3.170 kg/s.

Table 5. Companions of maximum vertical displacement at the top of the aquifer.

Case	Injection Rate, (kg/s)	Aquifer	Maximum Vertical Displacement V_{max}, (cm)			
			1 Y	5 Y	10 Y	30 Y
1	3.170	1	1.844	2.325	2.334	2.272
	0	2	−0.187	−0.078	−0.018	0.002
2	0	1	2.568	2.840	2.779	2.645
	3.170	2	1.062	1.064	1.036	0.998
3	1.585	1	2.147	2.681	2.683	2.634
	1.585	2	0.516	0.582	0.583	0.552
4	3.170	1	3.227	3.408	3.430	3.317
	3.170	2	0.724	0.725	0.701	0.683

In addition, a comparison between Case 3 and Case 4 reveals that in the case of multi-layer injection, increasing the CO_2 injection rate leads to larger vertical displacements in the aquifer, thereby increasing the risk of CO_2 leakage.

It should be noted that due to the low-permeability mudstone caprocks, the aquifer layers in the numerical model are hydraulically isolated, which explains why the CO_2 migration distance in Case 4 (5300 m after 30 years of injection) is close to the sum of Cases 1 and 2 (5050 m). However, even in the absence of hydraulic communication, the mechanical response of the formation remains continuous across layers. Pressure buildup in one aquifer induces additional mechanical loading on the overlying and underlying strata, contributing to cumulative vertical displacement at the surface. As a result, Case 4 exhibits greater uplift (3.317 cm in Aquifer 1) than the displacements in Cases 1 and 2 (2.272 cm and 2.645 cm, respectively).

6. Coulomb Failure Stress (*CFS*)

In general, a high injection rate can enhance CO_2 storage capacity but also increase the pore pressure in the aquifer, potentially causing fractures in the aquifers and caprocks, thereby increasing the risk of CO_2 leakage. Therefore, it is necessary to determine a reasonable injection rate based on considering both the safety of caprocks and the storage of the aquifers. In this research, the Coulomb Failure Stress (*CFS*) was selected as the indicator to identify the impact of injection rate on the safety of the aquifers and caprocks during numerical simulations. The points *A*, *B*, *C*, and *D* marked in Figure 2 were selected to monitor the *CFS* changes at the top of Caprock 1, Aquifer 1, Caprock 2, and Aquifer 2, respectively. The results are shown in Figure 6.

It is found that the *CFS* values at the top of each layer reach their peak in the first three years of injection. As the injection time increases, the pore pressure gradually stabilizes, causing the *CFS* value to stabilize as well. It is also found that the maximum *CFS* for Cases 1 to 3 is 0.591, 0.567, and 0.555, respectively, which suggests that the multi-layer injection method is safer than the single-layer injection method for CO_2 storage.

Figure 6 also reveals that at the same injection rate, CO_2 storage in deep layers results in lower *CFS* compared to shallow layers, indicating that deep aquifers have a lower risk of failure and are more suitable for CO_2 storage. For example, In Case 1, single-layer injection into the shallow aquifer leads to a maximum *CFS* of 0.591, whereas in Case 2, single-layer injection into the deeper aquifer results in a lower maximum *CFS* of 0.567.

Additionally, it can be observed that the higher the injection rate, the higher the *CFS* values. For example, in Cases 3 and 4, with injection rates of 1.585 and 3.17 kg/s, the peak *CFS* values are 0.555 and 0.595, respectively. Therefore, it is necessary to set a reasonable injection rate in practical engineering.

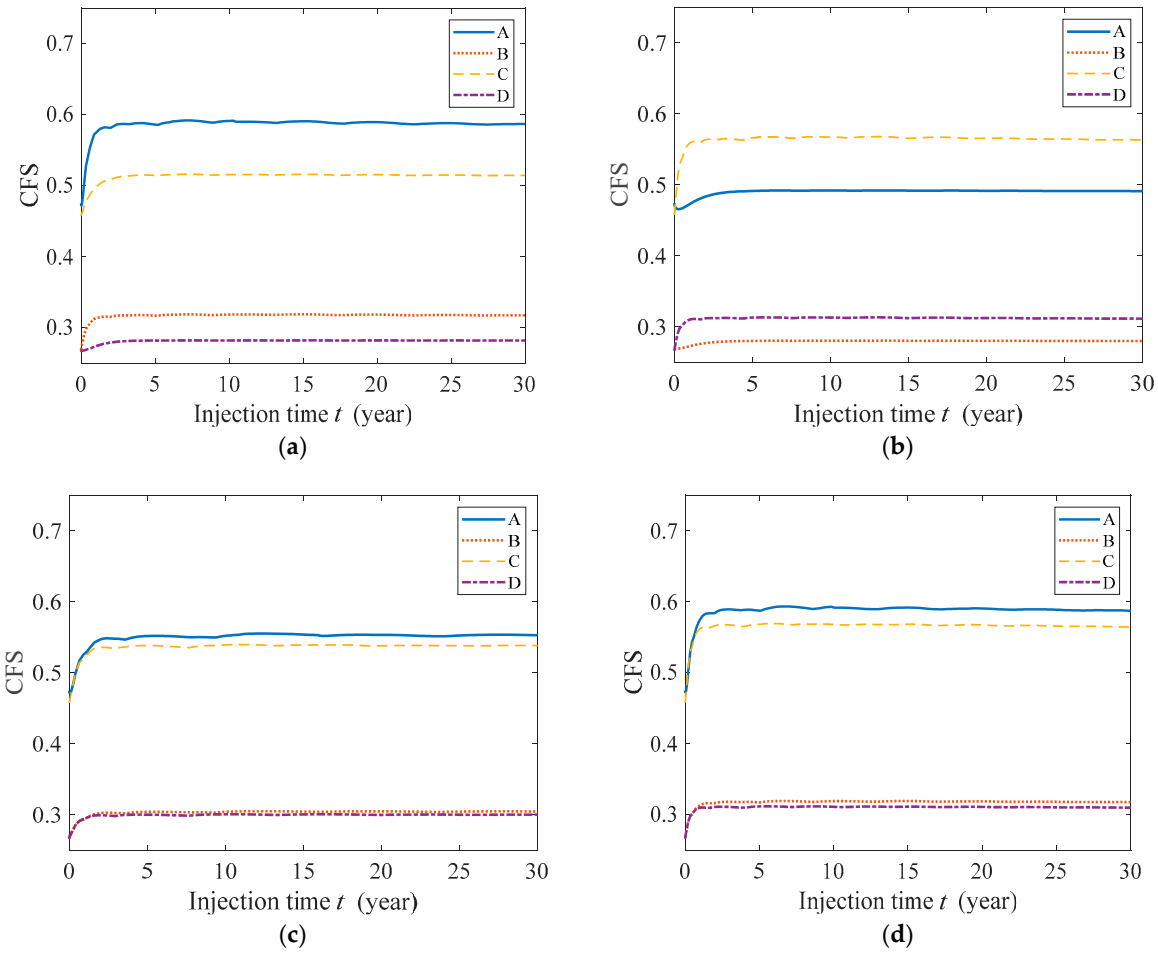


Figure 6. *CFS* curves of monitoring points under different injection scenarios. (**a**) Case 1, (**b**) Case 2, (**c**) Case 3, (**d**) Case 4.

Figure 7 compares the maximum *CFS* values at storage sites under different injection cases. The results indicate that, compared with other cases, Case 3 exhibits the lowest *CFS* value during the injection process, which also suggests that multi-layer injection offers enhanced stability compared to single-layer injection when the CO_2 injection volume is constant.

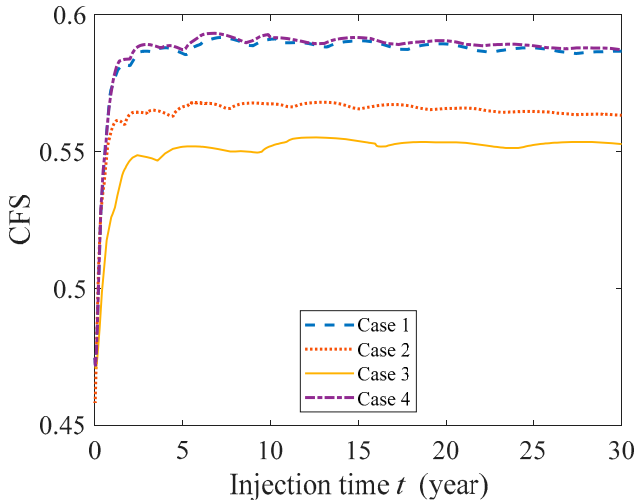


Figure 7. Comparison of the maximum *CFS* values under different injection conditions.

7. Limitations

In this study, a simplified 2D cross-sectional hydromechanical model was adopted, which was sufficient to capture the pressure-driven mechanical responses during CO_2 injection. Nevertheless, the 2D approach cannot fully represent the three-dimensional (3D) heterogeneity and lateral connectivity of geological formations, which may affect the spatial distributions of pore pressure, CO_2 saturation, and deformation at the field scale.

The aim of this study was to compare the performance of the multi-layer and the single-layer CO_2 injection methods under representative geological conditions of the East China Sea Shelf Basin. The numerical model used fixed mechanical and geometrical parameters derived from site-specific and literature-based data. However, the absence of a sensitivity analysis limits the ability to quantify the relative influence of geological factors (e.g., permeability and mechanical parameters) and operational parameters (e.g., injection rate) on CO_2 migration, pore pressure evolution, and geomechanical stability. Therefore, future research need to incorporate systematic sensitivity analyses, which will provide valuable insights into the robustness of the simulation outcomes.

In addition, although deeper saline aquifers demonstrate better CO_2 storage performance and geomechanical stability in this simulation, it is important to note that the associated drilling costs also increase significantly with depth. From an engineering and economic perspective, such cost implications may limit the practical feasibility of deep formations for CCS applications. Therefore, future site selection and injection planning should balance technical performance with cost-effectiveness.

8. Conclusions

Numerical analyses were carried out to investigate CO_2 migration behavior and the safety of geological formations under the multi-layer and the single-layer injection methods for offshore CO_2 saline aquifer storage. The main findings are summarized as follows:

(1) The use of the multi-layer injection method enhances CO_2 migration within saline aquifers, enabling a more efficient utilization of storage space compared with the single-layer injection method. After 1 year of injection, the combined CO_2 migration distance across two aquifers in Case 3 is 610 m, which is greater than that obtained in the single-layer injection in Cases 1 and 2 (350 m and 380 m, respectively).

(2) CO_2 storage in deep saline aquifers results in lower *CFS* values and exhibits superior CO_2 storage performance compared with that in shallow saline aquifers. After 30 years of injection in Cases 1 and 2, the maximum *CFS* values are 0.591 and 0.567, and the CO_2 migration distances are 2400 m and 2650 m, respectively.

(3) The injection rate plays an important role in balancing the storage efficiency of reservoirs and the geomechanical safety of caprocks. After 30 years of CO_2 injection, the migration distances in Aquifer 1 for Case 3 and Case 4 are 1500 m and 2400 m, and the maximum *CFS* values are 0.555 and 0.595, respectively.

Overall, the multi-layer injection strategy, particularly when applied to deep saline aquifers, presents a safer and more effective approach for large-scale offshore CCS projects. From an engineering perspective, the results of this study provide practical guidance for offshore CCS site selection and injection planning.

Author Contributions: Conceptualization, J.S. and Y.H.; methodology, J.S., F.M. and Y.H.; software, F.M.; validation, F.M. and J.S.; formal analysis, J.S. and F.M.; investigation, J.S. and F.M.; resources, Q.L., Y.H. and T.X.; writing—original draft preparation, J.S.; writing—review and editing, J.S., F.M. and Y.H.; supervision, T.X., Q.L. and Y.H.; project administration, T.X., Q.L. and Y.H.; funding acquisition, J.S. and Y.H. All authors have read and agreed to the published version of the manuscript.

Funding: This study was funded by National Natural Science Foundation of China (U24A20609 and 42477144) and the Science Foundation of Donghai Laboratory (DH-2022ZY0007).

Institutional Review Board Statement: Not applicable.

Informed Consent Statement: Not applicable.

Data Availability Statement: The data used to support the findings and results of this study are available from the corresponding author upon request.

Conflicts of Interest: Tao Xuan and Qi Li are employed by CNOOC Energy Development Co. Ltd. Engineering Technology Branch Tianjin and China Energy Engineering Group Zhejiang Electric Power Design Institute Co. Ltd., respectively. The remaining authors declare that the research was conducted in the absence of any commercial or financial relationships that could be construed as a potential conflict of interest.

References

1. Cui, Y.; Bai, J.; Liao, S.; Cao, S.; Liu, F. Suggestions on the development of environmental monitoring technology of CO_2 geological storage and leakage under the background of China's "Double-Carbon" strategy. *Atmosphere* **2023**, *14*, 14010051. [CrossRef]
2. Rasool, M.H.; Ahmad, M.; Ayoub, M. Selecting geological formations for CO_2 storage: A comparative rating system. *Sustainability* **2023**, *15*, 15086599. [CrossRef]
3. Aminu, M.; Nabavi, S.; Rochelle, C.; Manovic, V. A review of developments in carbon dioxide storage. *Appl. Energy* **2017**, *208*, 1389–1419. [CrossRef]
4. Martin-Roberts, E.; Scott, V.; Flude, S.; Johnson, G.; Haszeldine, R.S.; Gilfillan, S. Carbon capture and storage at the end of a lost decade. *One Earth* **2021**, *4*, 1569–1584. [CrossRef]
5. Bashir, A.; Ali, M.; Patil, S.; Aljawad, M.S.; Mahmoud, M.; Al-Shehri, D.; Hoteit, H.; Kamal, M.S. Comprehensive review of CO_2 geological storage: Exploring principles, mechanisms, and prospects. *Earth-Sci. Rev.* **2024**, *249*, 104672. [CrossRef]
6. Lin, Z.; Kuang, Y.; Li, W.; Zheng, Y. Research status and prospects of CO_2 geological sequestration technology from onshore to offshore: A review. *Earth-Sci. Rev.* **2024**, *258*, 104928. [CrossRef]
7. Li, L.; Liu, Y.; Li, Y.; Wang, Z.; Guo, K.; Ma, Q.; Cui, Y.; Liu, K.; Chen, C. Overview of typical projects for geological storage of CO_2 in offshore saline aquifers. *Liquids* **2024**, *4*, 744–767. [CrossRef]
8. Luo, D.; Yuan, Y.; Chen, J.; Li, Q.; Liang, J.; Zhao, H. Structural and reservoir characteristics of potential carbon dioxide storage sites in the Northern South Yellow Sea Basin, Offshore Eastern China. *J. Mar. Sci. Eng.* **2024**, *12*, 12101733. [CrossRef]
9. Zhao, J.; Zheng, J.; Ren, L.; Lin, R.; Zhou, B. A review on geological storage of marine carbon dioxide: Challenges and prospects. *Mar. Pet. Geol.* **2024**, *163*, 106757. [CrossRef]
10. Kumar, S.; Foroozesh, J.; Edlmann, K.; Rezk, M.; Lim, C. A comprehensive review of value-added CO_2 sequestration in subsurface saline aquifers. *J. Nat. Gas Sci. Eng.* **2020**, *81*, 103437. [CrossRef]
11. Qin, J.; Zhong, Q.; Tang, Y.; Rui, Z.; Qiu, S.; Chen, H. CO_2 storage potential assessment of offshore saline aquifers in China. *Fuel* **2023**, *341*, 127681. [CrossRef]
12. Yu, J.; Pei, J.; Xu, J. New insight into oil and gas exploration in Miocene and Late Oligocene strata in Qiongdongnan basin. *J. Earth Sci.* **2009**, *20*, 811–823. [CrossRef]
13. Lu, P.; Hao, Y.; Bai, Y.; Liu, W.; Chen, X.; Zheng, H.; Liu, J.; Chen, Y.; Gao, J. Optimum selection of favorable areas for CO_2 geological storage in the Majiagou Formation in the Ordos Basin. *Int. J. Greenh. Gas Control* **2021**, *109*, 103360. [CrossRef]
14. Bohloli, B.; Skurtveit, E.; Choi, J.; Grande, L.; Sauvin, G.; Soldal, M.; Wilkinson, H. Determination of shear properties and evaluation of fracture reactivation for a clay-rich shale: A case study from Svalbard, Arctic Norway. *Bull. Eng. Geol. Environ.* **2020**, *79*, 4859–4872. [CrossRef]
15. Shukla, R.; Ranjith, P.; Haque, A.; Choi, X. A review of studies on CO_2 sequestration and caprock integrity. *Fuel* **2010**, *89*, 2651–2664. [CrossRef]
16. Rutqvist, J.; Tsang, C.F. A study of caprock hydromechanical changes associated with CO_2-injection into a brine formation. *Environ. Geol.* **2002**, *42*, 296–305. [CrossRef]
17. Gholami, R.; Raza, A.; Iglauer, S. Leakage risk assessment of a CO_2 storage site: A review. *Earth-Sci. Rev.* **2021**, *223*, 103849. [CrossRef]
18. Wijaya, N.; Morgan, D.; Vikara, D.; Grant, T.; Liu, G. Basin-scale study of CO_2 storage in stacked sequence of geological formations. *Sci. Rep.* **2024**, *14*, 18661. [CrossRef] [PubMed]
19. Zhu, Q.; Zuo, D.; Zhang, S.; Zhang, Y.; Wang, Y.; Wang, L. Simulation of geomechanical responses of reservoirs induced by CO_2 multilayer injection in the Shenhua CCS project, China. *Int. J. Greenh. Gas Control* **2015**, *42*, 405–414. [CrossRef]

20. Shi, L.; Bai, B.; Wu, H.; Li, X. Evaluating reservoir risks and their influencing factors during CO_2 injection into multilayered reservoirs. *Geofluids* **2017**, *2017*, 6059142. [CrossRef]
21. Liu, H.; Hou, Z.; Were, P.; Gou, Y.; Sun, X. Simulation of CO_2 plume movement in multilayered saline formations through multilayer injection technology in the Ordos Basin, China. *Environ. Earth Sci.* **2014**, *71*, 4447–4462. [CrossRef]
22. Kivi, I.R.; Makhnenko, R.Y.; Oldenburg, C.M.; Rutqvist, J.; Vilarrasa, V. Multi-Layered systems for permanent geologic storage of CO_2 at the gigatonne scale. *Geophys. Res. Lett.* **2022**, *49*, 100443. [CrossRef]
23. Wei, X.; Li, Q.; Li, X.; Niu, Z. Modeling the hydromechanical responses of sandwich structure faults during underground fluid injection. *Environ. Earth Sci.* **2016**, *75*, 1155. [CrossRef]
24. Jiang, Z.; Li, Y.; Du, H.; Zhang, Y. The Cenozoic structural evolution and its influences on gas accumulation in the Lishui Sag, East China Sea Shelf Basin. *J. Nat. Gas Sci. Eng.* **2015**, *22*, 107–118. [CrossRef]
25. Sun, L.; Zhang, J.; Zhang, T.; Yan, X.; Chen, T.; Liu, J. Paleosalinity reconstruction for the Paleocene sequence of Lishui Sag in the East China Sea Shelf Basin. *Arab. J. Sci. Eng.* **2022**, *47*, 7433–7448. [CrossRef]
26. Teng, J.; Fu, Q.; Qin, J.; Ma, W.; Zhang, G.; Feng, K. Quantitative evaluation of Paleocene reservoir diagenetic facies by logging in Lishui West Sag, East China Sea Basin. *Minerals* **2024**, *14*, 28. [CrossRef]
27. Zhu, Z.; Qi, L.; Chen, H.; Li, J.; Zhang, Y.; Qin, J.; Zhao, Y.; Ni, C. Tectono-stratigraphic evolution in the Paleocene Lishui Sag, East China Sea Shelf Basin. *Aust. J. Earth Sci.* **2024**, *71*, 439–456. [CrossRef]
28. Li, Y.; Zhang, J.; Xu, Y.; Chen, T.; Liu, J. Improved understanding of the origin and accumulation of hydrocarbons from multiple source rocks in the Lishui Sag: Insights from statistical methods, gold tube pyrolysis and basin modeling. *Mar. Pet. Geol.* **2021**, *134*, 105361. [CrossRef]
29. Rutqvist, J.; Wu, Y.; Tsang, C.F.; Bodvarsson, G. A modeling approach for analysis of coupled multiphase fluid flow, heat transfer, and deformation in fractured porous rock. *Int. J. Rock. Mech. Min.* **2002**, *39*, 429–442. [CrossRef]
30. Kim, T.; Park, C.H.; Watanabe, N.; Park, E.S.; Park, J.W.; Jung, Y.B.; Kolditz, O. Numerical modeling of two-phase flow in deformable porous media: Application to CO_2 injection analysis in the Otway Basin, Australia. *Environ. Earth Sci.* **2021**, *80*, 121. [CrossRef]
31. Basmanov, O.L.; Kiryukhin, A.V.; Maguskin, M.A.; Dvigalo, V.N.; Rutqvist, J. Thermo-hydrogeomechanical modeling of vertical ground deformation during the operation of the Mutnovskii Geothermal Field. *J. Volcanol. Seismol.* **2016**, *10*, 138–149. [CrossRef]
32. Qi, L.; Zhang, Y. Numerical simulation analysis of parameters in an artificial gas cap of CO_2 enhanced oil recovery and storage. *Chem. Technol. Fuels Oil* **2025**, *61*, 258–267. [CrossRef]
33. Chen, B.; Li, Q.; Tan, Y.; Zhang, Y.; Yu, T.; Ma, J.; Zhong, Y.; Li, X. Caprock sealing integrity and key indicators of CO_2 geological storage considering the effect of hydraulic-mechanical coupling: X field in the Bohai Bay Basin, China. *Eng. Geol.* **2024**, *342*, 107741. [CrossRef]
34. Liu, L.; Li, Y.; Dong, H.; Sun, Z. Diagenesis and reservoir quality of Paleocene tight sandstones, Lishui Sag, East China Sea Shelf Basin. *J. Petrol. Sci. Eng.* **2020**, *195*, 107615. [CrossRef]
35. Gercek, H. Poisson's ratio values for rocks. *Int. J. Rock. Mech. Min.* **2007**, *44*, 1–13. [CrossRef]
36. Blanco-Martín, L.; Jahangir, E.; Rinaldi, A.P.; Rutqvist, J. Evaluation of possible reactivation of undetected faults during CO_2 in-jection. *Int. J. Greenh. Gas Control* **2022**, *121*, 103794. [CrossRef]
37. Figueiredo, B.; Tsang, C.F.; Rutqvist, J.; Bensabat, J.; Niemi, A. Coupled hydro-mechanical processes and fault reactivation induced by CO_2 injection in a three-layer storage formation. *Int. J. Greenh. Gas Control* **2015**, *39*, 432–448. [CrossRef]
38. Cappa, F.; Rutqvist, J.; Yamamoto, K. Modeling crustal deformation and rupture processes related to upwelling of deep CO_2-rich fluids during the 1965-1967 Matsushiro earthquake swarm in Japan. *J. Geophys. Res-Solid Earth* **2009**, *114*, B10304. [CrossRef]
39. Ren, B.; Littlefield, J.; Jia, C.; Ni, H.; Duncan, L. Impact of pressure-dependent interfacial tension and contact angle on capillary heterogeneity trapping of CO_2 in storage aquifers. *SPE J.* **2024**, *29*, 4442–4458. [CrossRef]
40. Stavropoulou, E.; Laloui, L. Evaluating CO_2 breakthrough in a shaly a caprock material: A multi-scale experimental approach. *Sci. Rep.* **2022**, *12*, 10706. [CrossRef] [PubMed]
41. Kim, Y.H.; Park, Y.G. A review of CO_2 plume dispersion modeling for application to offshore carbon capture and storage. *J. Mar. Sci. Eng.* **2024**, *12*, 38. [CrossRef]
42. Harris, R.A. Introduction to special section: Stress triggers, stress shadows, and implications for seismic hazard. *J. Geophys. Res-Solid Earth* **1998**, *103*, 24347–24358. [CrossRef]
43. Wang, Q.; Zhang, D.; Li, Y.; Li, C.; Tang, H. Numerical simulation study of CO_2 storage capacity in deep saline aquifers. *Sci. Technol. Energy Tr.* **2024**, 79. [CrossRef]

Disclaimer/Publisher's Note: The statements, opinions and data contained in all publications are solely those of the individual author(s) and contributor(s) and not of MDPI and/or the editor(s). MDPI and/or the editor(s) disclaim responsibility for any injury to people or property resulting from any ideas, methods, instructions or products referred to in the content.